Electronic Supplementary Material (ESI) for Journal of Materials Chemistry C.

Supporting information.

Magnetic interplay between two different lanthanides in a tris-phthalocyaninato complex: a viable synthetic route and detailed investigation in bulk and on surface.

Yanhua Lan,*[a] Svetlana Klyatskaya,*[a] Mario Ruben,[ab] Olaf Fuhr,[ac] Wolfgang Wernsdorfer,[de] Andrea Candini,[f] Valdis Corradini,[f] Alberto Lodi Rizzini,[g] Umberto del Pennino,[g] Filippo Troiani,[f] Loïc Joly,[b] David Klar,[h] Heiko Wende,[h] and Marco Affronte[fg]

AUTHOR ADDRESS

[a] Institute of Nanotechnology (INT), Karlsruhe Institute of Technology (KIT), 76344 Eggenstein-Leopoldshafen, Germany

[b] Universite de Strasbourg, Institut de Physique et de Chimie des Materiaux de Strasbourg, Campus de Cronenbourg, 23 Rue du Loess, 67034 Strasbourg Cedex 2, France

[c] *Karlsruhe Nano Micro Facility* (KNMF), Karlsruhe Institute of Technology (KIT), 76344 Eggenstein-Leopoldshafen, Germany

[d] Univ. Grenoble Alpes, Inst NEEL, 25 rue des Martyrs, F-38000 Grenoble, France

[e] CNRS, Inst NEEL, F-38000 Grenoble, France

[f] CNR Institute of Nanoscience S3 via G. Campi 213A, 41125 Modena, Italy

[g] Università di Modena e Reggio Emilia, Dipartimento di Fisica, Informatica, Matematica, via G. Campi 213A, 41125 Modena, Italy

[h] Faculty of Physics and Center for Nanointegration Duisburg-Essen (CENIDE), University of Duisburg-Essen, Lotharstraße 1, D-47048 Duisburg, Germany

Contents:

General synthetic remarks. Reactions requiring an inert gas atmosphere were conducted under argon, and the glassware was oven dried (140°C). All reagents were purchased from commercial sources and used as received. Radial chromatography was performed on Chromatotron 7924T, with plates prepared from Silica gel $60PF_{254}$ containing gypsum. 1,2–Dicyano-4,5-di(hexyl)benzene (**3**), lithium salt of phthalocyanine with eight hexyl groups (**4**) and lanthanide bis-phthalocinines $LnPc_2$ (**5**, **6**) were prepared according to the literature procedures.[Klyatskaya S., Eichhöfer A., Wernsdorfer, J. Inorg. Chem., 2014, 4179–4185, Branzoli F., Carretta P., Filibian M., Klyatskaya S., Ruben M. Phys.Rev.B, 82(17), 2011, 174419; Phys. Rev. B, 82(13), 2010, 134401/1-134401]

General Procedure for the Synthesis of $PcLn_1PcLn_2Pc$* (1, 2).

Under a slow stream of Ar, a mixture of twenty milligrams of Li_2Pc* (**4**) and 80 mg of $Ln(acac)_3$ and 5 mL of 1-chloconaphthalene, percolated throught a basic alumina column just before being used, were put in a 10 mL round flask equipped with a condenser. The mixture was heated on an oil bath set at 60 °C with mechanical stirring until the entire solid was dissolved. Then 20 mg of Pc_2Ln_1 were added and the bath temperature was increased, and the mixture continued refluxing for 3 h with careful monitoring by UV spectrum. The reaction solution was cooled to room temperature, and 80 mL of methanol was added. The precipitant was filtered, washed with methanol, and extracted with dichloromethane. The extract solution was chromatographed on a silica gel column (Silica Gel 60, Kanto Chemicals, particle size 40-60 μm). Using dichloromethane as an eluent, we eluted a green band of unreacted Pc_2Ln initially. The second blue-green band of the aimed substance was collected. The solution was concentrated, methanol was added, and the solution was filtered. The chromatographic separation was repeated until the band of unreacted Pc_2Ln disappeared. The final product $PcLn_1PcLn_2Pc$* was obtained as a blue-black powder (typically 25 mg). The compounds were identified by MALDI-ToF.

Ln_1= Dy, Ln_2=Tb (**1**). The complex **1** was separated from the crude mixture by column chromatography (basic alumina oxide), eluting with CH_2Cl_2/MeOH (10:1) followed by reprecipitation from the hexane/CH_2Cl_2 mixture to afford a deep green solid of neutral **1** (28 mg, 24% yield from **4**; R_f = 0.38; CH_2Cl_2). MALDI-ToF calculated for $C_{144}H_{144}DyN_{24}Tb$ ($M\text{-}H^+$): 2531.0708. Found 2531.6706 (M^+, 100 %).

Ln_1=Ln_2=Y (**2**). The complex **2** was separated from the crude mixture by column chromatography (basic alumina oxide), eluting with CH_2Cl_2/MeOH (10:1) followed by reprecipitation from the hexane/ CH_2Cl_2 mixture to afford a deep green solid of neutral **3** (24 mg, 20% yield from **4**; R_f = 0.38; CH_2Cl_2). MALDI-ToF calculated for $C_{144}H_{144}N_{24}Y_2$ ($M\text{-}H^+$): 2387.0160. Found 2387.6942 (M^+, 100 %).

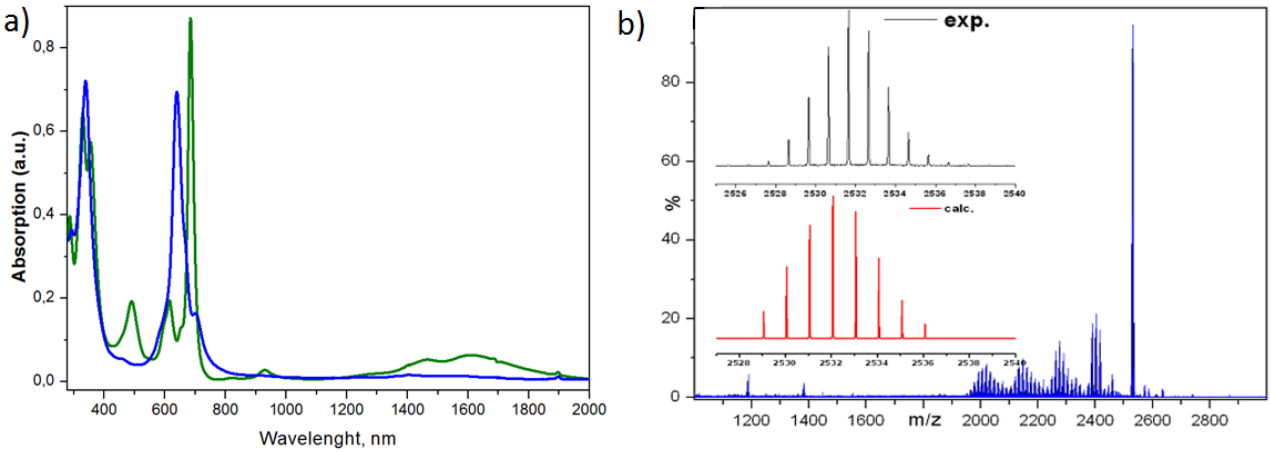

Figure S1. Complex $PcLn_1PcLn_2Pc$*, Ln_1 =Dy, Ln_2=Tb. a) UV-Vis/Nir-IR spectra of complex **1** (blue) and for comparison of $[TbPc_2]^0$ (green), measured at room temperature, $CHCl_3$. b) MALDI ToF spectra of complex **1**; where the experimental and calculated (red lines) values of the relative abundances of the isotopic ions are summarized.

X-Ray crystallography. Crystals suitable for single crystal X-ray diffraction were obtained by slow diffusion of EtOH into a solution of complex **1** in hexane and then selected in perfluoroalkylether oil. Single-crystal X-ray diffraction data of **1** were collected using graphite-monochromatised MoKα radiation (λ = 0.71073 Å) on a STOE IPDS2T diffractometer. Raw intensity data were collected and treated with the STOE X-Area software Version 1.64. Data were corrected for Lorentz and polarisation effects. Interframe Scaling was done with the implemented program LANA.

The structure was solved with the direct methods program SHELXS of the SHELXTL PC suite programs,[G. M. Sheldrick, *SHELXTL PC version 5.1*, Bruker Analytical X-ray Systems, Karlsruhe, 2000] and was refined with the use of the full-matrix least-squares program SHELXL. Crystal data and the results of the refinement are collected in Table 1. Molecular diagrams were prepared using Diamond.[Diamond Version 2.1d, K. Brandenburg, Crystal Impact GbR, 1996-2000]

In **1** Tb, Dy and all C and N atoms were refined with anisotropic displacement parameters. Two of the hexyl groups showed strong disorder which was modelled using partial-occupancy carbon atoms. Disordered C atoms were refined isotropically. H atoms were placed in fixed positions. Solvent C_6H_{14} was also refined with partial occupancy.

CCDC-1054639 (**1**) contains the supplementary crystallographic data for this paper. These data can be obtained free of charge at www.ccdc.cam.ac.uk/ (or from the Cambridge Crystallographic Data Centre, 12 Union Road, Cambridge CB2 1EZ, UK; fax: (internat.) +44-1223/336-033).

Table S1. Crystallographic data for compound (**1**).

	1.C_6H_{14}
Elemental formula[a]	$C_{144}H_{144}DyN_{24}Tb$
Formula weight, [g/mol]	2618.41
Crystal system	monoclinic
Space group	$P2_1/c$
Unit cell dimensions	
a, b, c, [Å]	26.4588(6), 20.8628(6), 24.7745(7)
α, β, γ, [°]	90, 109.148(2), 90
Cell volume, V,[Å^3]	12919.0(6)
Calculated density, [Mg/m^3]	1.346
No. of formula units/cell, Z	4
F(000)	5428
Absorption coefficient, μ(λ), [mm^{-1}]	1.179
Temperature, [K]	180
Total No. of reflections measured	50953
No. of unique reflections measured	21335
R_{int} for equivalents	0.0460
No. of "observed" reflections , I>2σ_I	12466
Parameters/restraints	1533/44
Goodness of fit	0.849
Final *R* indices, R_1 ("observed" data)[b], wR_2 (all data)[c]	R_1 = 0.0392; wR_2 = 0.0961
Largest diff. peak/hole, [e Å^{-3}]	0.736 / -0.605

[a] Non-integer numbers of atoms result from partial disorder of the hexyl groups which could not be completely modeled; [b] $R_1 = \Sigma||F_o| - |F_c||/\Sigma|F_o|$; [c] $wR_2 = \{\Sigma[w(F_o^2-F_c^2)^2] / \Sigma[w(F_o^2)^2]\}^{1/2}$

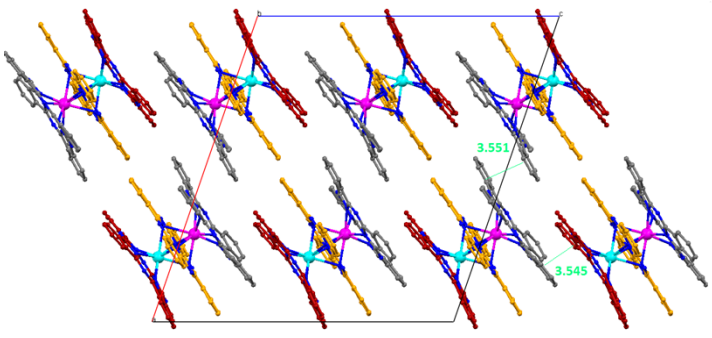

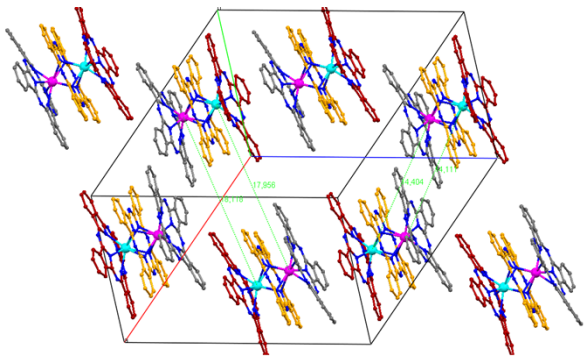

Fig. S2 Packing diagram of **1**. Solvent molecules located between the n-hexyl chains and the n-hxexyl chains have been omitted for clarity. A pi–pi stack arrangement within columns along the *a* axis (left). Each molecule of **1** is rather well separated from neighboring molecules by the n-hexyl chains. The intermolecular Tb–Dy distances: 1.440 nm, 1.795-1.811 nm (right).

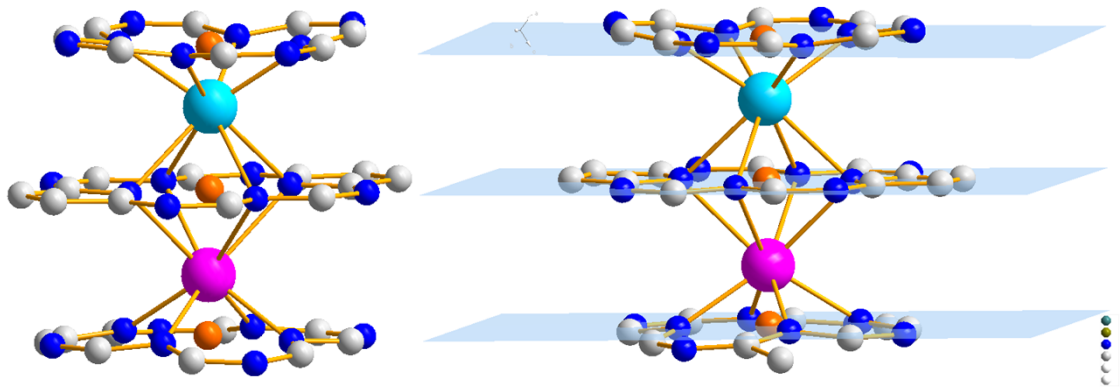

Fig. S3a. The central unit of the molecule of **1**. The orange atom is a dummy atom defined by the four donor atoms of nitrogen in each layer of Pc/Pc* ring. The twist angel is calculated as a torsion angel from one N donor and the dummy atom of one plane through the Ln atom then to the corresponding N donor of another plane. The angel between the top Pc ring to the center Pc ring is calculated as 45.83, 46.76, 46.49 and 46.40°; the average angel comes to 46.4°. The angel between the bottom Pc* ring to the center Pc ring is calculated as 32.0, 32.3, 32.5 and 31.9°; the average angel comes to 32.2°.

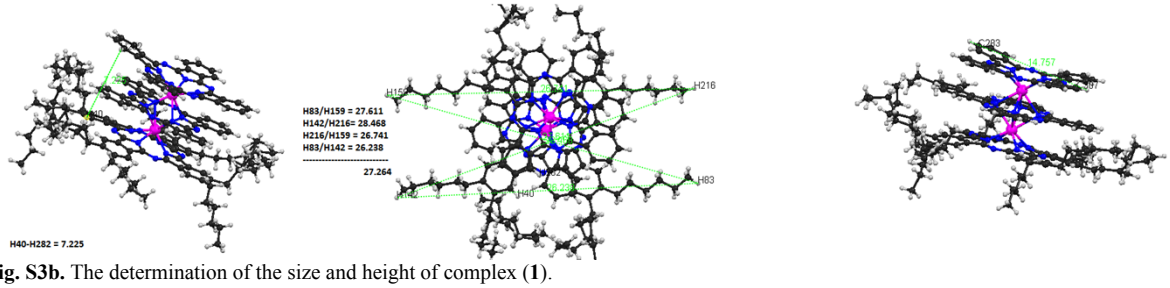

Fig. S3b. The determination of the size and height of complex (**1**).

Bulk magnetic data

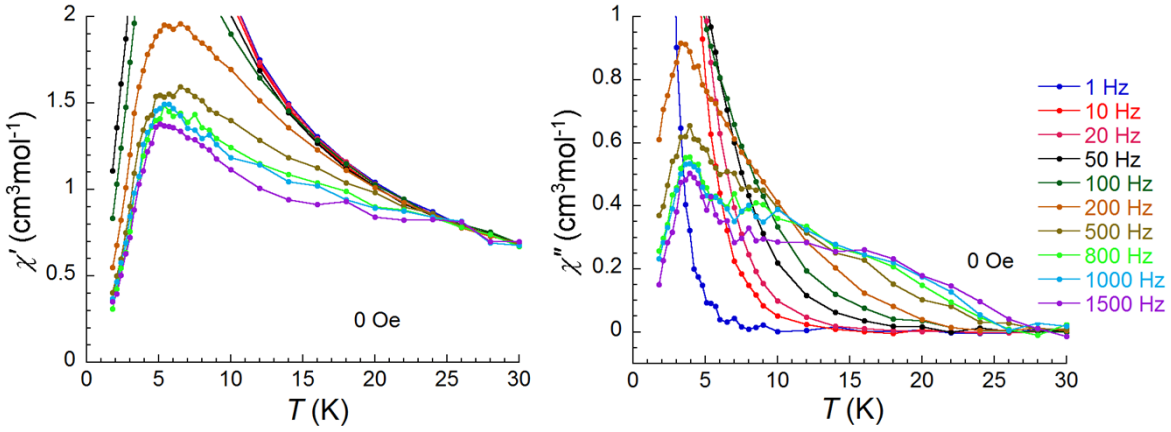

Figure S4a.Temperature dependence of the in-phase and out-of-phase components of the ac magnetic susceptibility at different frequencies for **1** under zero dc field (in zoom view to the high temperature range).

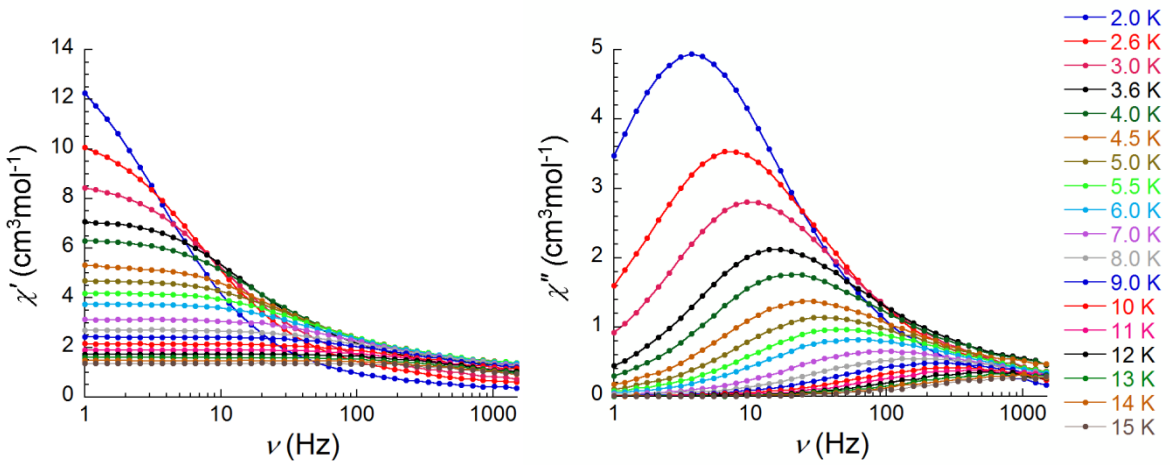

Figure S4b. Frequency dependence of the in-phase (left) and the out-of-phase (right) components of the ac susceptibility at different temperatures for **1** under zero dc field.

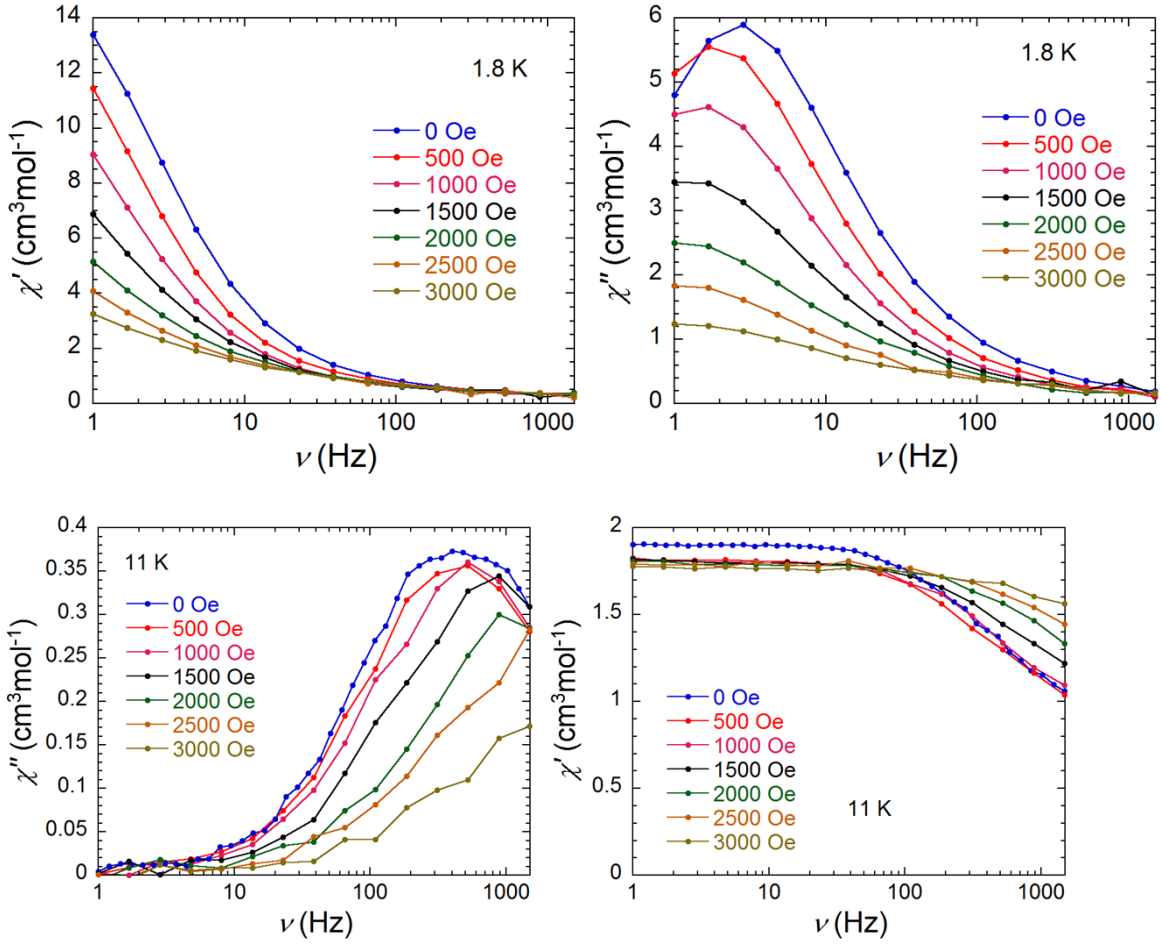

Figure S5. Frequency dependence of the in-phase (left) and out-of-phase (right) components of the ac magnetic susceptibility for **1** under applied dc fields at 1.8 K (top) and 11 K (down).

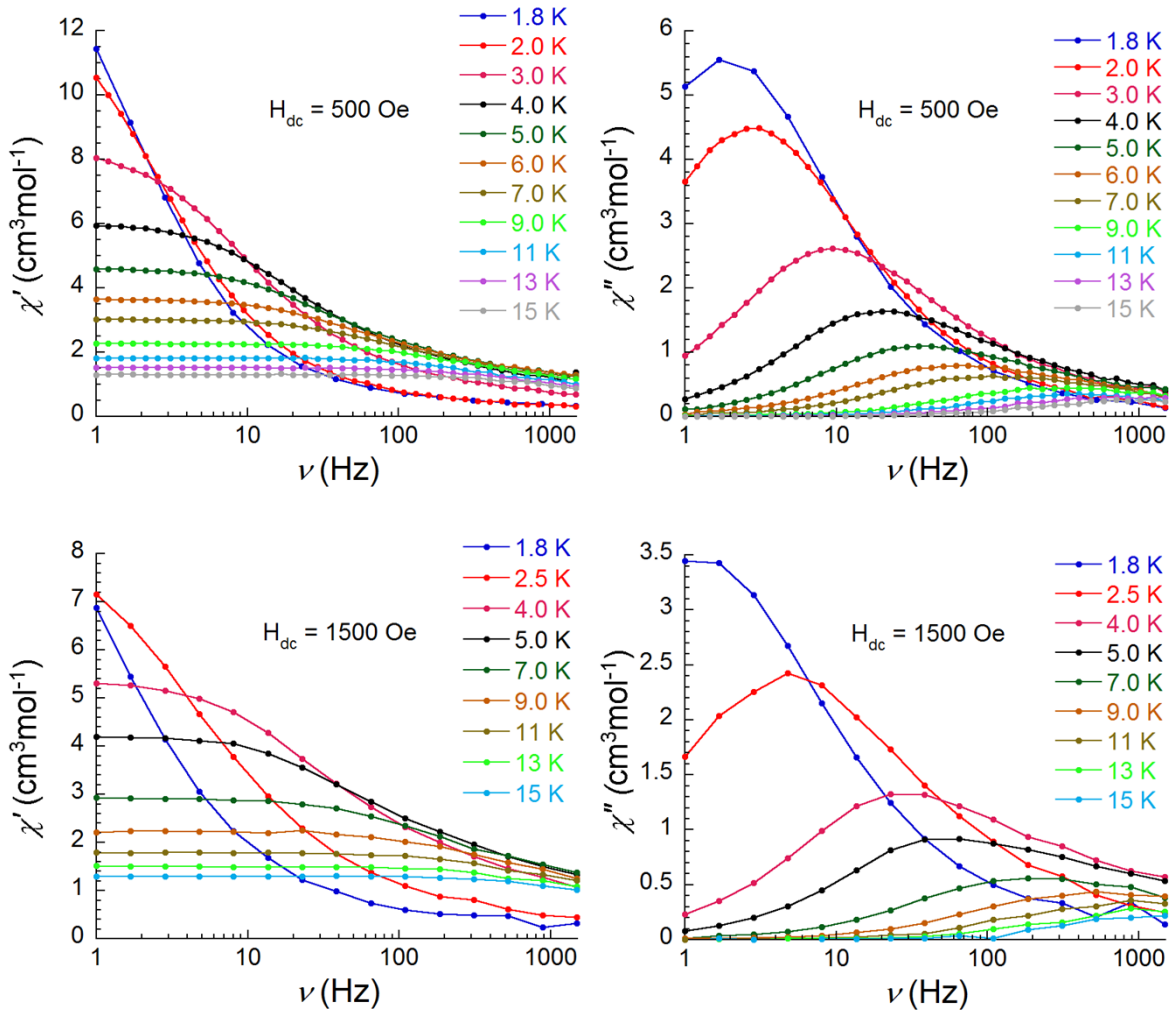

Figure S6. Frequency dependence of the in-phase (left) and out-of-phase (right) components of the ac magnetic susceptibility at different temperatures for **1** under an applied dc field of 500 Oe (top) and 1500 Oe (down).

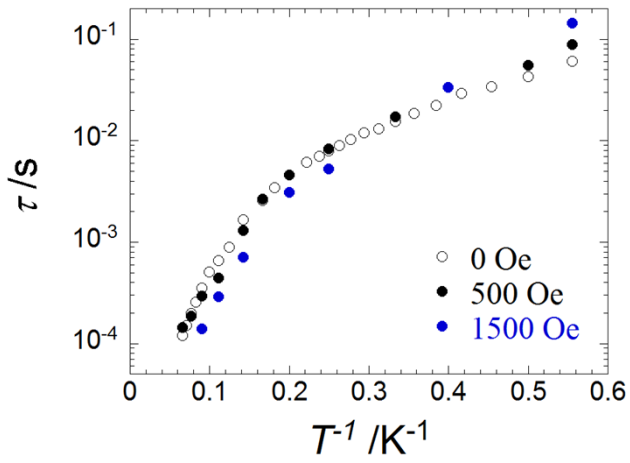

Figure S7. Field dependence of the relaxation time τ as a function of 1/T under a DC field of 0, 500 and 1500 Oe, which are almost superposed to the same slope.

The ac frequency dependent measurements were also performed under an applied dc field (Figure S6). As depicted in Figure S7, the relaxation rates with the application of different strength of dc fields sligtly deviate from the slope under zero field. This behaviour suggests that small -but finite- quantum tunnelling effects, that are certainly active below 1K (see below), are also operative at higher temperature.

Table S2: Parameters obtained from fitting of Cole-Cole diagram of compound **1**.

T (K)	α	χ_0 (cm^3/mol)	χ_{inf} (cm^3/mol)	R^2
2.0	0.260(0)	15.23(6)	0.353(9)	0.999
3.0	0.284(10)	9.20(6)	0.67(46)	0.980
4.0	0.304(15)	6.62(4)	1.04(4)	0.942
5.0	0.276(14)	4.81(2)	1.23(3)	0.954
6.0	0.273(15)	3.83(1)	1.19(2)	0.957
7.0	0.237(17)	3.17(1)	1.16(2)	0.954
8.0	0.242(13)	2.73(1)	1.09(2)	0.977
9.0	0.204(14)	2.43(0)	1.05(2)	0.979
10	0.240(13)	2.16(0)	0.94(2)	0.984
11	0.171(13)	1.91(0)	0.87(2)	0.987
12	0.134(16)	1.74(0)	0.88(2)	0.979
13	0.220(14)	1.61(0)	0.70(2)	0.987

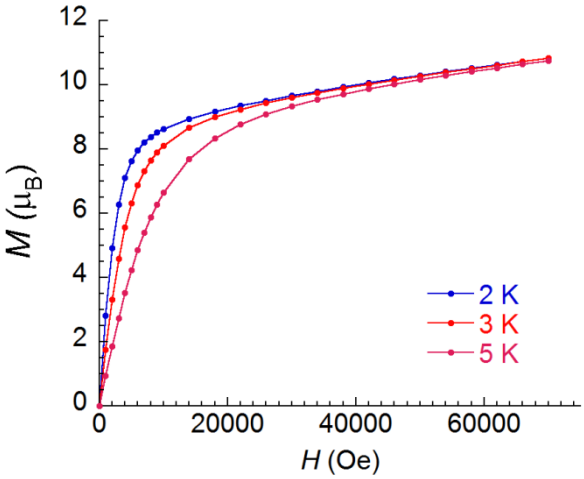

Figure S8. Field dependence of magnetization of **1** at indicated temperatures.

The field-dependence of the magnetization rises abruptly to reach *ca.* 9 μ_B up to 10 kOe, which is consistent with the presence of ferromagnetic interactions. Above 10 kOe, the magnetization curve increases in a linear fashion to reach 10.8 μ_B with a lack of saturation even at 70 kOe. This is indicative of the presence of magnetic anisotropy as a result of Dy^{3+} and Tb^{3+} ions.

microSQUID measurements.

100% TD compound 1

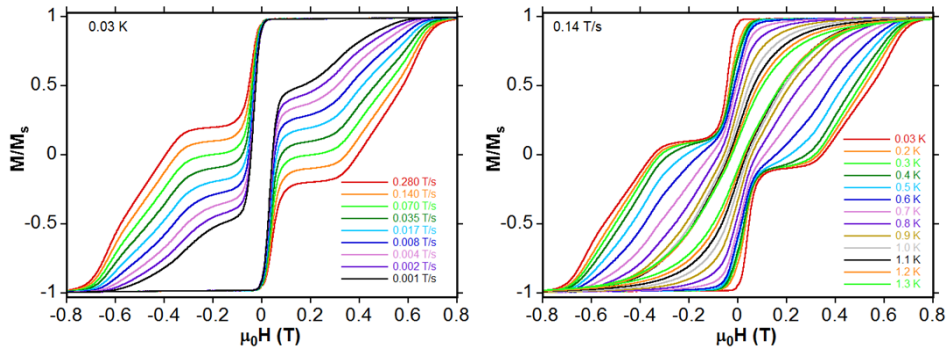

1% diluted TD

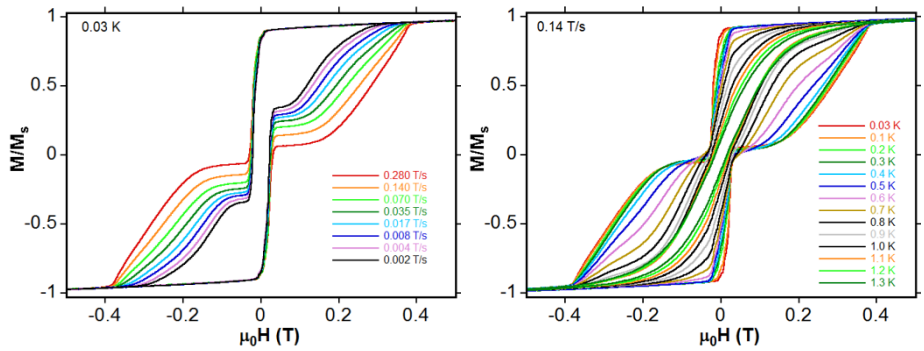

Figure S9. Sweep rate dependence (left) and temperature dependence (right) of magnetization curves taken on derivative **1** and 1% of **1** diluted in PcYPcYPc*.

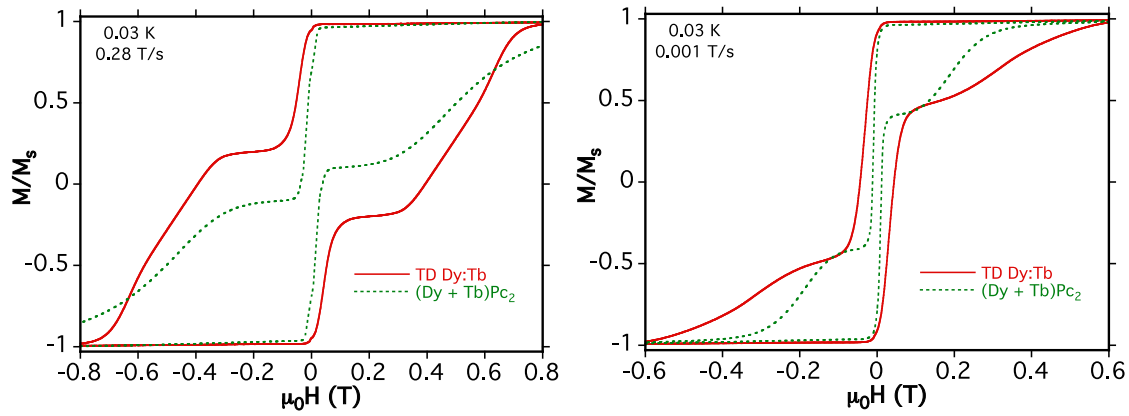

Figure S10a. For comparison, plots for 100% sample. Isothermal magnetization curve taken at 0.03K and with 'fast' (0.280 T/s) and "slow" sweeping rate (0.001T/s) on derivative **1.** The M(H) curve measured on isolated $TbPc_2$ and $DyPc_2$ double decker (the sum of the two contribution) is also plotted for comparison.

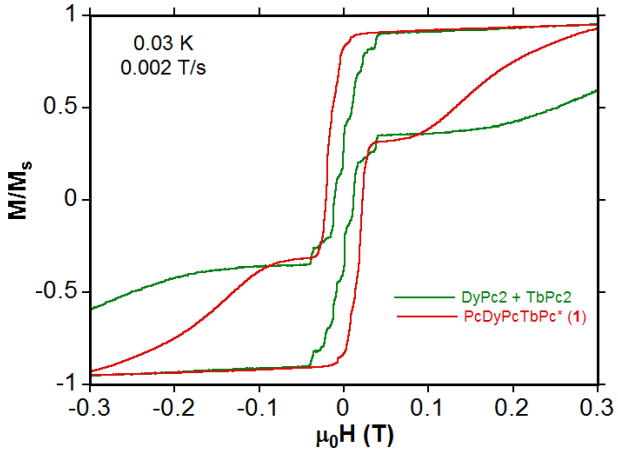

Figure 10b. **For comparison, plots for diluted samples.** Magnetization measured as function of applied magnetic field at 0.03 K and sweeping rate (0.002 T/s). Opening of hysteresis loop is evident with characteristic step-like behavior due to blocking of magnetization and fast relaxation due to quantum tunneling in 1% PcDyPcTbPC* (**1**) diluted in PcYPcYPc* (red line). The sum of the magnetization of double decker 2% $TbPc_2$ and 2% $DyPc_2$ diluted in YPc_2 is also plotted for comparison (green dotted curve).

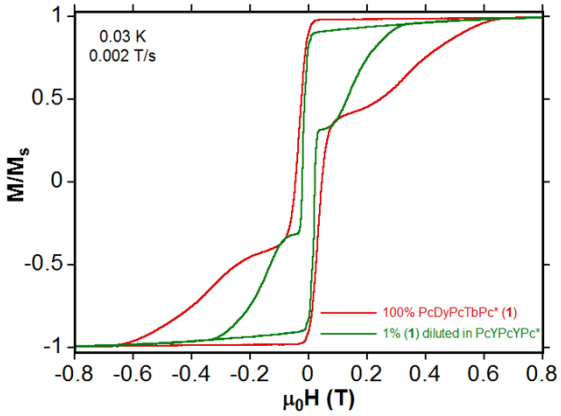

Figure 10c. **For comparison, plots for 100% sample and diluted samples.** Magnetization measured as function of applied magnetic field at 0.03 K and sweeping rate (0.002 T/s). Opening of hysteresis loop is evident with characteristic step-like behavior due to blocking of magnetization and fast relaxation due to quantum tunneling in both PcDyPcTbPC* (**1**) (red line) and 1% (**1**) diluted in PcYPcYPc* (green line).

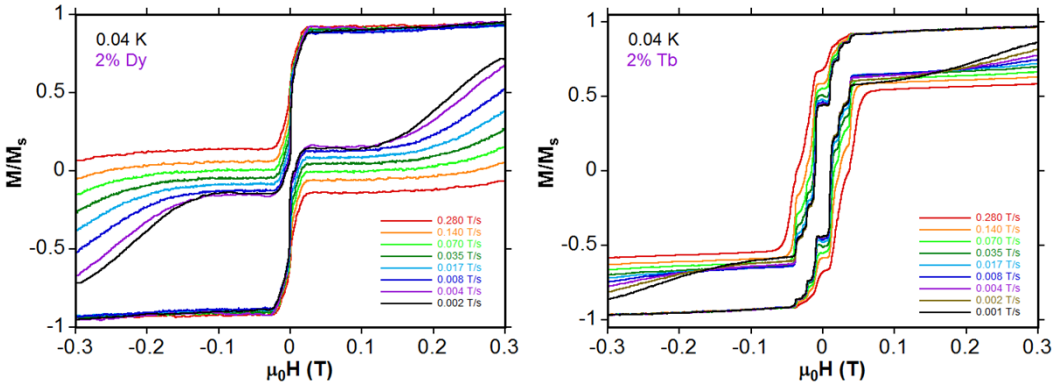

(a) (b)

Figure S11. Sweep rate dependent magnetization curves taken at 0.04 K on isolated 2% of $DyPc_2$ (left, a) and 2% of $TbPc_2$ (right, b) diluted in YPc_2 double decker.

Heat Capacity.

The Schottky anomaly is accounted by the expression:

$$\frac{C_S}{R} = \frac{g_0}{g_1}\left(\frac{T_0}{T}\right)^2 \frac{\exp\left(\frac{T_0}{T}\right)}{\left[1+\frac{g_0}{g_1}\exp\left(\frac{T_0}{T}\right)\right]^2}$$

in which $k_B T_0$ is the effective energy interaction between two equally degenerated ($g_0 = g_1$) spins.

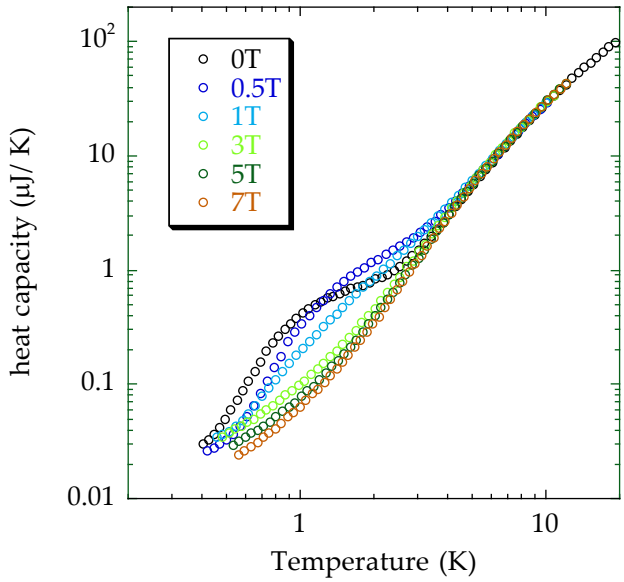

Figure S12. Magnetic field dependence of heat capacity of derivative **1.**

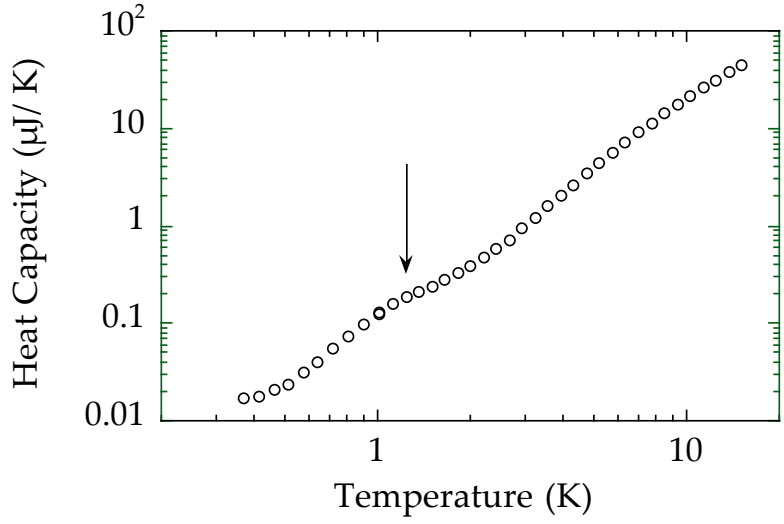

Figure S13. Heat capacity of derivative **1** diluted in 90% non-magnetic PcYPcYPc. Notice that the position of the maximum of Schottky anomaly is essentially identical of that measured in non diluted **1** derivative suggesting that inter-molecular dipolar interaction are not particularly relevant.

Surface analysis.

Integrity check by XPS and stoichiometry. STM. Surface coverage.

STM was used to check that the two dimensional distribution of molecules. Room temperature STM image acquisition was carried out in constant current mode with typical conditions of 2.0 V and the lowest achievable current (30 pA) in order to minimize dragging and damaging of the soft organic materials by the scanning tip. Using optimal deposition conditions, STM images (see Fig. S14b) show nanometer size spots with no evidence of 3D aggregation.

From a statistical analysis of the STM images, we derived that approximately 10–30% of the surface was covered by **1** molecules (see Table S3). From the STM line-profiles (Figure S14c), we reproducibly found an average lateral size of 2.5 ± 1.0 nm and a height of 0.6 ± 0.2 nm, close to the dimensions of the single molecule (diameter of 2.0 nm and height of 0.6 nm), convoluted with the dimension of the tip.

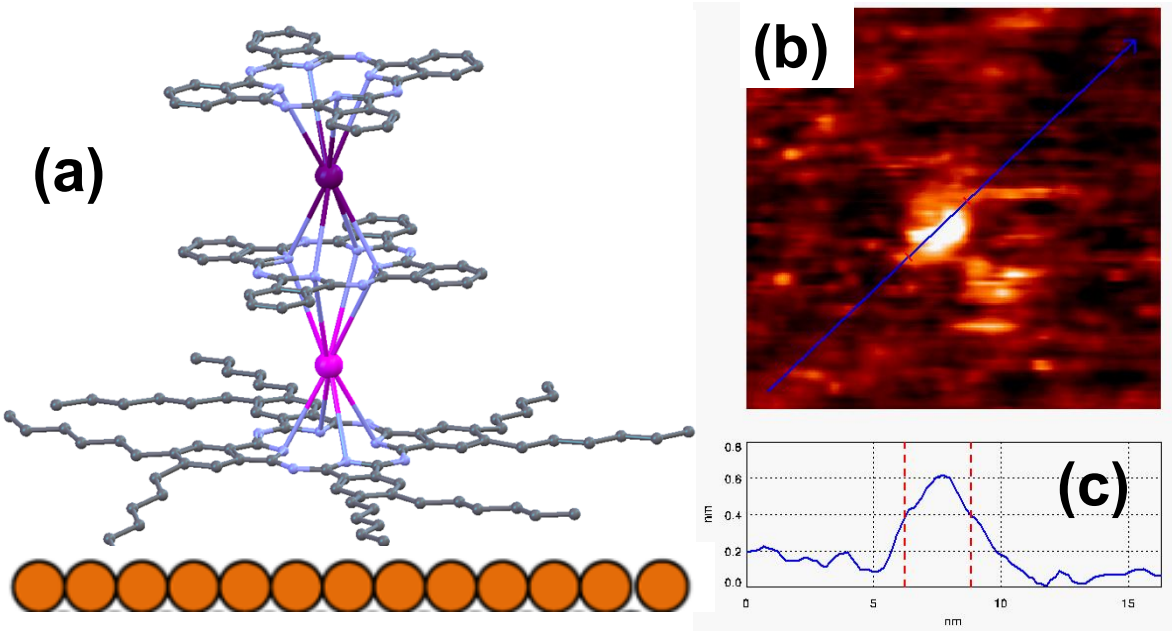

Figure S14. (a) Molecular structure of the **1** molecule deposited on the surface. (b) STM image (12 nm × 12 nm) (2.0 V, 30 pA) of a sub-ML of deposited on Au(111) surface, and (c) line-profiles taken along the directions indicated.

XPS investigation.

In figure S15 the Tb-3d, Dy-3d and N-1s core level spectra of the **1** deposited from liquid-phase on the Au(111) and HOPG surfaces are plotted along with their line shapes nicely reproduce the corresponding ones obtained on thick film (TF). For quantitative analysis of XPS spectra we used conventional method reported in textbooks (Handbook of X-ray Photoelectron Spectroscopy Published by, Perkin-Elemer Corporation, 1979, and references therein; Practical Surface Analysis: Auger and X-Ray Photoelectron Spectroscopy by D. Briggs, M.P. Seah, Second Edition (1990). Modern ESCA The Principles and Practice of X-Ray Photoelectron Spectroscopy by T. L. Barr, CRC Press, Inc. (1994). An introduction to surface analysis by XPS and AES by J. F. Watts and J. Wolstenholme (John Wiley & Sons Chichester England 2003); MAE 649 Microscopy and Spectroscopy database Chapter 3: X-ray Photoelectron Spectroscopy)

In particular the XPS peak intensity I_A (=peak area) of an element A:

$$I_A = n_A K T L_A \sigma_A \lambda \cos\vartheta$$

with:

n_A =atomic concentration of the element

K = instrument constant

T= transmission function of the analyser

L_A= angular asymmetry factor of orbital

σ = the photoionization cross section of the i-peak

λ = inelastic mean free path length

θ = emission angle

is used to evaluate the stoichiometry ratio between different elements. For all core levels the line shapes of the ML's and TF are quite similar. The stoichiometric ratios Tb-3d/Dy-3d, N-1s/ Dy-3d and C-1s/Dy-3d are reproducible (see Table S3) and close to the expected ones (1, 24 and 144 respectively), proving the chemical stability of the molecular core.

From the Tb-4f/ Au-3d ratio (and taking into account the attenuation of gold signal due to the overlayer) we derive the Tb,Dy-TD coverage reported in Table S3, in agreement with the values obtained from STM.

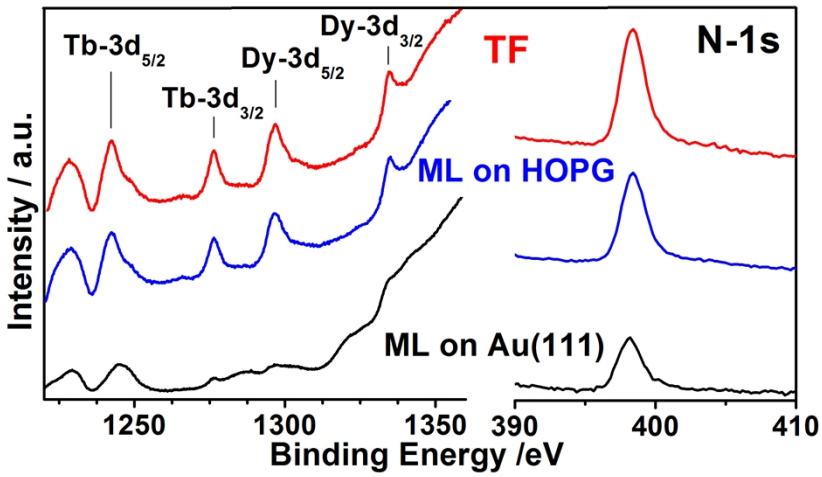

Figure S15. XPS core level spectra obtained after immersing, for 10min in 10^{-5}M solution of **1**, the the Au(111) substrate (black lines), the HOPG (blue line). The corresponding spectra taken on the thick films (red line) are shown for comparison.

Table S3. Stoichiometric ratios derived from the core level intensities of the Tb,Dy-TD MLs deposited from liquid-phase on the Au(111) and HOPG surfaces and the corresponding thick film TF. The stoichiometric values expected from the structural characterization are reported in squared brackets.

Derivative	Time & conc	Substrate	Rinse	Tb-3d/Dy-3d [1]	N-1s/Dy-3d [24]	C-1s/ Dy-3d [144]	Coverages	
							XPS	STM
ML	10' in 10^{-5}M	Au(111)	10''		26 ± 5	190 ± 50	**25-35%**	**10-30%**
ML	10' in 10^{-5}M	HOPG	No	1.01 ± 0.05	23 ± 5		**40-50%**	
TF	1 Drop 10^{-5}M	HOPG		0.99 ± 0.05	22 ± 5			

XAS and XMCD.

- **XMCD-spectra at 0°**

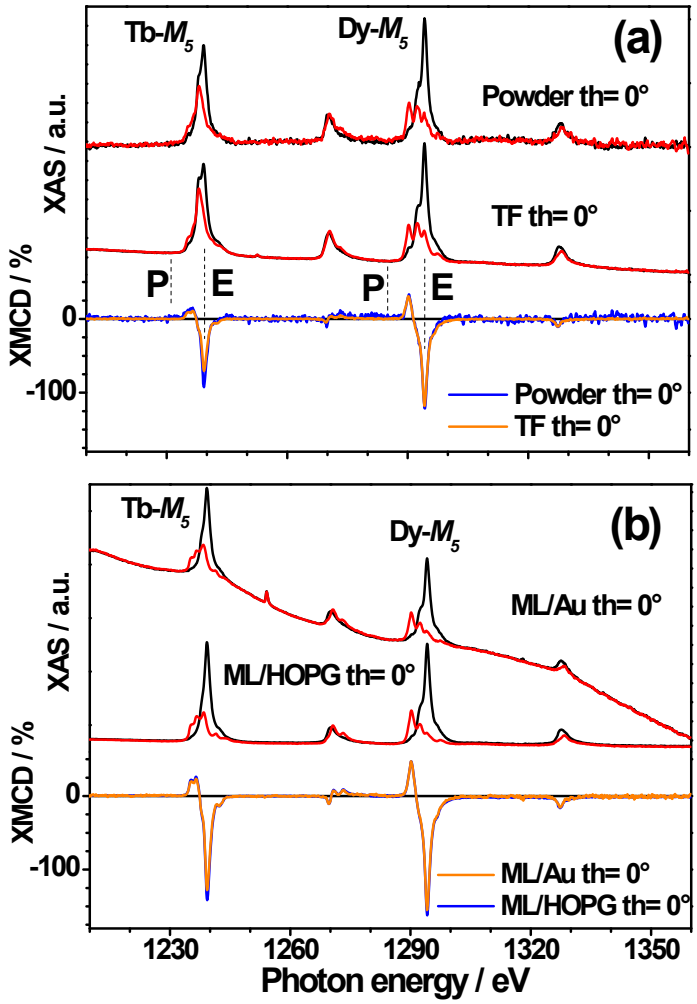

Figure S16. (a) XAS and the circular dichroism (lower panels) at the Tb and Dy $M_{4,5}$ edges measured for the Tb,Dy-TD TF compared with the corresponding Powder. (b) XAS and the circular dichroism (lower panels) at the Tb and Dy $M_{4,5}$ edges measured for the ML on HOPG compared with the ML on Au. All the measurement are performed at normal incidence (θ =0°). E and P represent the edge and pre-edge positions for a fast detection of the dichroic signal (see discussion in the manuscript).

- **XMCD-spectra at 0° vs 60° : oriented molecules with axis perp. to surface.**
-

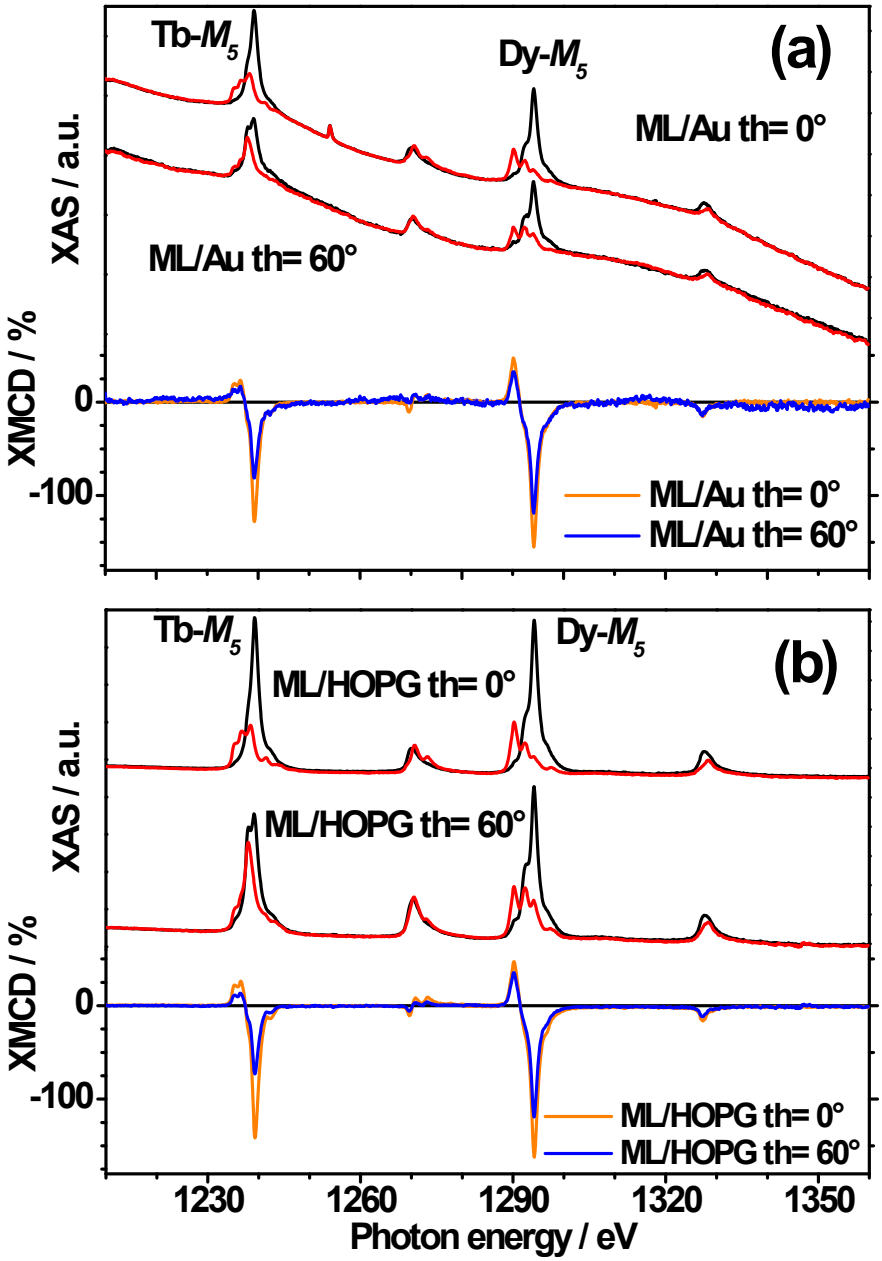

Figure S17. X-ray Absorption spectra (upper panels) and the circular dichroism (lower panels) at the Tb and Dy $M_{4,5}$ edges measured for the ML on Au(111) (a) and the ML on HOPG (b). Two different angles are compared (θ =0° and θ =60°).

- **XLD -spectra at 60° : oriented molecules with axis perp. to surface.**

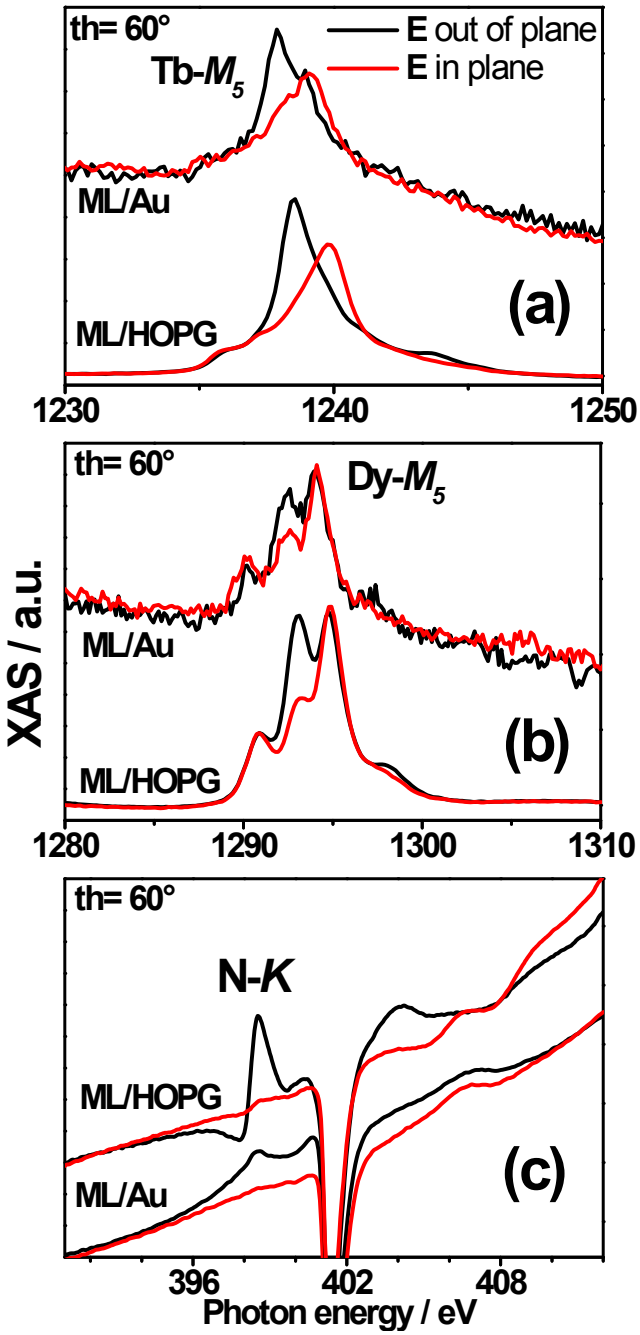

Figure S18. X-ray linear dichroism at the (a) Tb M_5, (b) Dy M_5, and (c) N K edges at θ =60°. The Tb,Dy-TD ML on Au(111) (upper panels) and the ML on HOPG (lower panels) are compared. The huge absorption dip at about 402eV is due to the presence of a nitrogen contamination on the mirror.

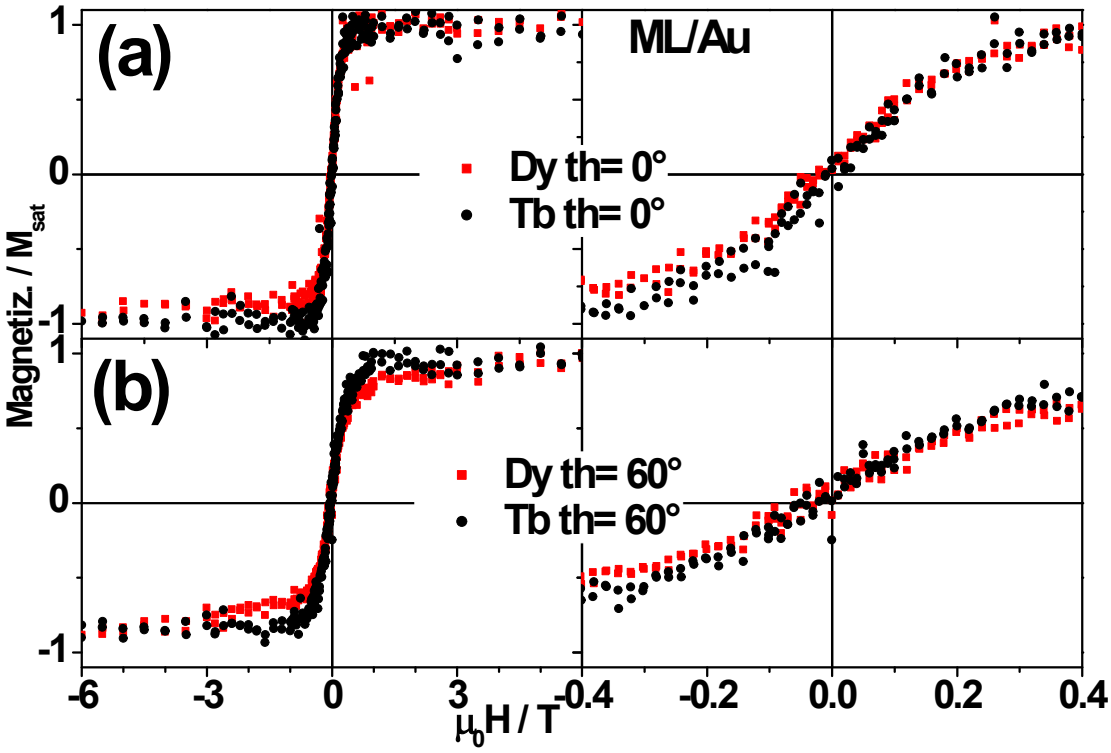

Figure S19. Magnetization loop derived by the XMCD signal measured at the Tb and Dy M_5 edges respectively at 1.8K as function of applied magnetic field. PcDyPcTbPc* have been dispersed on Au(111) substrate and lie with one Pc flat on the substrate. The external magnetic field was applied at an angle θ = 0° (a) and θ = 60°(b) with respect to the Au surface. The panels on the right are a zoom in the low field region.

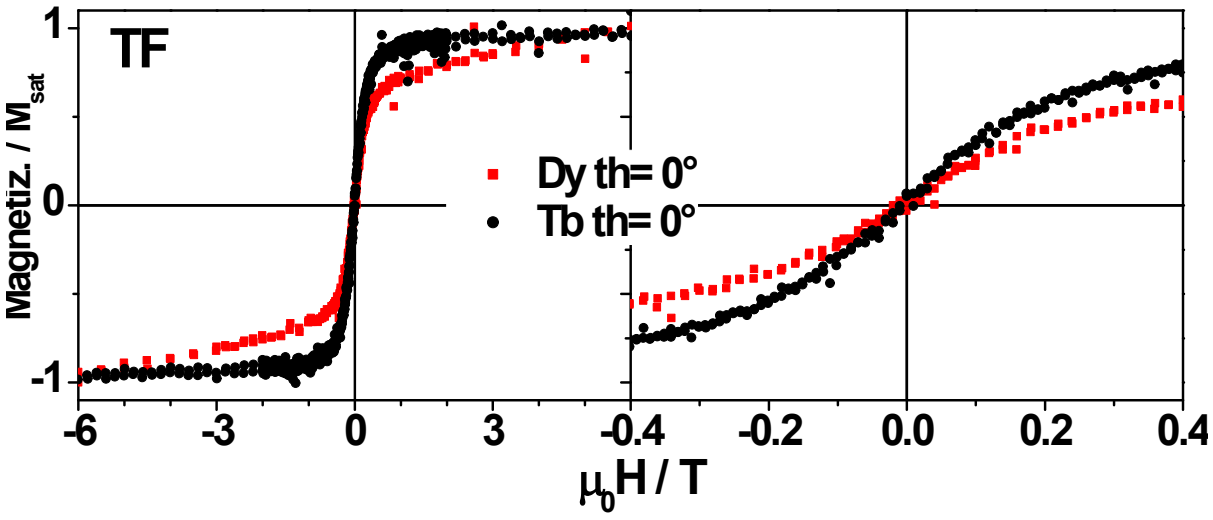

Figure S20. Magnetization loop derived by the XMCD signal measured at the Tb and Dy M_5 edges respectively at 1.8K as function of applied magnetic field for the PcDyPcTbPc* Thick Film. The external magnetic field was applied at an angle θ = 0°. The panels on the right are a zoom in the low field region.